

Video Article

Creating Dynamic Images of Short-lived Dopamine Fluctuations with Ip-ntPET: Dopamine Movies of Cigarette Smoking

Evan D. Morris^{1,2,3,4}, Su Jin Kim^{1,3}, Jenna M. Sullivan^{1,3,4}, Shuo Wang^{3,4}, Marc D. Normandin⁵, Cristian C. Constantinescu⁶, Kelly P. Cosgrove^{1,2,3}¹Diagnostic Radiology, Yale University²Psychiatry, Yale University³Yale PET Center, Yale University⁴Biomedical Engineering, Yale University⁵Nuclear Medicine, Massachusetts General Hospital⁶Radiological Sciences, University of California, IrvineCorrespondence to: Evan D. Morris at evan.morris@yale.eduURL: <https://www.jove.com/video/50358>DOI: [doi:10.3791/50358](https://doi.org/10.3791/50358)

Keywords: Behavior, Issue 78, Neuroscience, Neurobiology, Molecular Biology, Biomedical Engineering, Medicine, Anatomy, Physiology, Image Processing, Computer-Assisted, Receptors, Dopamine, Dopamine, Functional Neuroimaging, Binding, Competitive, mathematical modeling (systems analysis), Neurotransmission, transient, dopamine release, PET, modeling, linear, time-invariant, smoking, F-test, ventral-striatum, clinical techniques

Date Published: 8/6/2013

Citation: Morris, E.D., Kim, S.J., Sullivan, J.M., Wang, S., Normandin, M.D., Constantinescu, C.C., Cosgrove, K.P. Creating Dynamic Images of Short-lived Dopamine Fluctuations with Ip-ntPET: Dopamine Movies of Cigarette Smoking. *J. Vis. Exp.* (78), e50358, doi:10.3791/50358 (2013).

Abstract

We describe experimental and statistical steps for creating dopamine movies of the brain from dynamic PET data. The movies represent minute-to-minute fluctuations of dopamine induced by smoking a cigarette. The smoker is imaged during a natural smoking experience while other possible confounding effects (such as head motion, expectation, novelty, or aversion to smoking repeatedly) are minimized.

We present the details of our unique analysis. Conventional methods for PET analysis estimate time-invariant kinetic model parameters which cannot capture short-term fluctuations in neurotransmitter release. Our analysis - yielding a dopamine movie - is based on our work with kinetic models and other decomposition techniques that allow for time-varying parameters¹⁻⁷. This aspect of the analysis - temporal-variation - is key to our work. Because our model is also linear in parameters, it is practical, computationally, to apply at the voxel level. The analysis technique is comprised of five main steps: pre-processing, modeling, statistical comparison, masking and visualization. Preprocessing is applied to the PET data with a unique 'HYPR' spatial filter⁸ that reduces spatial noise but preserves critical temporal information. Modeling identifies the time-varying function that best describes the dopamine effect on ¹¹C-raclopride uptake. The statistical step compares the fit of our (Ip-ntPET) model⁷ to a conventional model⁹. Masking restricts treatment to those voxels best described by the new model. Visualization maps the dopamine function at each voxel to a color scale and produces a dopamine movie. Interim results and sample dopamine movies of cigarette smoking are presented.

Video Link

The video component of this article can be found at <https://www.jove.com/video/50358/>

Introduction

Despite overwhelming evidence of the medical risks, tobacco smoking is still a major health problem. It is simply very hard to quit smoking. Over 20% of the adult U.S. population continues to smoke and most smokers who attempt to quit relapse within the first month¹⁰. Unfortunately, there are few available treatments to aid in smoking cessation and/or reduce nicotine dependence. In our lab, we are interested in using PET imaging to understand addiction and dependence in order to aid in the development of new medications for smoking cessation and other drug-taking.

The rapid rise of dopamine in the striatum is believed to encode the addictive liability of drugs and behaviors¹¹ and the rapid return of dopamine to baseline may be related to withdrawal and subsequent drug-seeking. For some addictive substances and behaviors like cigarette smoking, the elevation of striatal dopamine is very short-lived (minutes); the magnitude of the rise is not large (1-2X baseline); and the spatial extent of these responses may be limited to small sub-regions of the striatum.

Animal experiments clearly demonstrate that nicotine causes dopamine release in the nucleus accumbens of rats¹². But early attempts - using conventional analyses - to estimate dopamine changes in humans during or following nicotine or smoking have yielded unreliable and contradictory results¹³⁻¹⁸. Some of these studies allowed smokers to smoke outside the scanner. Others delivered only nicotine to the subject. To best study addiction to cigarettes, we set out to develop better imaging protocols and complement them with advanced analyses that would allow us to capture the brain's response to a quasi-natural smoking behavior.

Positron Emission Tomography (PET) is unique among brain scanning techniques in its ability to probe the neurochemistry of the human brain *in vivo*. Many PET tracers exist to track dopamine receptors and many are susceptible to competition with endogenous dopamine. Unfortunately, the conventional methods of PET image analysis estimate the steady state ratio of bound to free tracer, known as binding potential (analogous to *in vitro* methods), from dynamic PET images. An *apparent* change in the steady state ratio (*e.g.* from the baseline to the smoking condition) is taken to indicate dopamine change. But the dopamine changes relevant to addiction are inherently *transient* so estimates of a steady-state quantity are flawed. Furthermore, the typical region-of-interest analysis averages the tracer concentration over large anatomically-defined regions and is likely to miss highly localized brain responses - such as those we expect from cigarette smoking. Previous PET studies of smoking may have also suffered from movement of the smokers' heads during smoking in the scanner.

Functional MRI (fMRI) offers the necessary spatial and temporal resolution that would be needed to capture events occurring in sub-regions of the striatum on the minute time-scale but fMRI lacks the molecular specificity of PET. The BOLD signal derives from changes in blood flow and is therefore neuronally and molecularly nonspecific. Thus, we utilized PET - but in a new way. The goal of this protocol was to estimate the brief and localized *dopamine responses* to smoking because they are believed to underlie the neurochemical manifestation of craving and drug-seeking behavior.

To estimate dopamine transients that are captured in dynamic PET images made with dopamine-receptor ligands, we previously introduced a series of kinetic models, collectively referred to as "ntPET" for neurotransmitter PET^{1,5,6,19}, that were based on the conventional two-tissue compartment model but were augmented by terms for the time-variation in dopamine and the interaction between dopamine and the tracer (*i.e.* competition). These models have been validated against a gold standard. Specifically, we have demonstrated that our models predict dopamine concentrations over time from PET data in rats that are in good agreement with simultaneously acquired microdialysis measurements^{4,7}. **Advantages:** The most recent of our models have been either linear and non-parametric (np-ntPET)¹ or linear and parametric (lp-ntPET)⁷. The latter model derives from an earlier linear model introduced by Alpert *et al.*²⁰. Linearization is a key development because it assures that applying the models to dynamic data at the voxel level is computationally simple. In a recent proof-of-concept paper, we were able to create dopamine movies of a human subject performing a motor task³ and show that the movies were sensitive to the timing of the motor task as would be expected. Movies are representations of the time course of dopamine levels at every voxel in an image. Voxel-by-voxel methods in PET generally suffer from low signal to noise ratio, so to minimize the noise inherent in voxel-based time-activity curves (TACs), we apply an innovative spatial filter, 'HYPR',⁸ as a pre-processing step. This step preserves key temporal characteristics of the responding voxels while reducing noise.

Smoking is more than nicotine delivery. Cigarettes contain 4,000 chemicals in addition to nicotine. While nicotine is thought to be primarily responsible for the initial addictive effects, all the other cues and sensory components of smoking become reinforcing to a habitual smoker. We chose to study the entire behavior of smoking which meant that we needed to be able to image smokers smoking while inside the PET scanner. Unfortunately, with smoking comes head motion. To eliminate head motion artifacts in our images, we use the Vicra motion-tracking system (NDI Systems, Waterloo, Canada) and event-by-event motion correction as part of an iterative, resolution recovery reconstruction algorithm²¹.

Our new scanning and analysis methods are designed to elicit and capture brief and localized dopamine transients that are the unique signatures of the brain's response to addictive drugs and behaviors. Performed voxel-by-voxel, our models produce a dynamic set of images of striatal dopamine fluctuations - *i.e.* "dopamine movies". These movies represent a new spatio-temporal biomarker of addiction and could serve as a direct, multi-dimensional indicator of risk for addiction and/or indicator of treatment efficacy.

Protocol

An outline of the entire procedure, described below, for producing multi-slice dopamine movies is summarized in the flow chart in **Figure 1**.

1. Pre-PET MR scan

Acquire a structural MR scan on a separate day from the PET scan. The MR scan will provide an anatomical reference for the PET images. Typical acquisition parameters for the structural MRI are: 3D MPRAGE MR pulse sequence with TE = 3.3 msec, flip angle = 7 degrees; slice thickness = 1.0 mm, 0.98 x 0.98 mm pixels.

1. Practice PET/Smoking Session

Arrange for the subject to practice the smoking motion in the PET scanner either before the scan or, ideally, on an earlier visit to the PET center. This will avoid confusion or discomfort during the actual PET scan. It will also eliminate the novelty of being in the scanner for the first time. Because the Siemens HRRT is a high resolution brain scanner, the tunnel is narrow and there is minimal clearance for the smoker to bring the cigarette to his/her mouth. Although we have a sophisticated system for addressing head motion, it is still advisable to have the smoker practice smoking while trying not to move his/her head.

2. Patient Prep

1. IV line

An IV must be inserted by a registered nurse and readied for later attachment to the pump that delivers the tracer. Tracer will be injected into the patient through an IV line.

2. Head Motion Monitor

Affix reflective spheres to the top of the head of the subject. The Vicra head-tracking system's lasers poll the position of reflective spheres at a rate of 20 Hz. The spheres are attached to rigid, cross-shaped "tool" and the tool is attached to a Lycra swim cap worn by the subject. A real-time display of the position of the tool should be used by the study personnel to monitor head motion and to make sure that the laser system has an unobstructed view of the tool and is recording the head position continually for later use in image reconstruction.

3. Prepare Injection Pump

1. Program the pump with proper infusion paradigm for raclopride To maximize sensitivity of the PET images to dopamine fluctuations throughout the scan, administer the tracer, ¹¹C-raclopride, as an initial bolus followed by a constant infusion. To determine the proper relative amounts of tracer to be delivered in the initial bolus vs. the infusion, we follow the method of Carson *et al.*²² to calculate the ratio of dose in the bolus to infusion rate ("Kbol" in units of minutes) given knowledge of the

impulse response function of ^{11}C -raclopride in humans. The delivery of tracer according to a given protocol is controlled by an in-house computer program that drives a programmable infusion pump.

4. Start Air Filter
To eliminate secondhand smoke from the PET suite during the smoking, position the intake of an air-filter (Movex Inc, Northampton, PA) in front of the scanner and above the subject's head. Leave room for a subject to bring the cigarette to his/her mouth during smoking. The filter is turned on prior to the study and is used in all conditions if multiple scans are performed.
 5. Transmission scan
Acquire a 9 min transmission scan prior to injection of tracer and acquisition of the PET scan. The transmission is acquired to create a 3D map of the linear attenuation coefficient throughout the brain. The attenuation map is used in the reconstruction of emission (PET) images.
2. PET Scan
 1. Start injection and PET scan
A certified nuclear medicine technologist must administer the tracer. Generally, a team of two technologists initiates tracer administration and PET data acquisition simultaneously.
 2. Rating scales at time of smoking
Administer simple questionnaires, orally, to the subject immediately prior to and following smoking. The smoker must rate his/her craving, satisfaction of craving, nicotine high, and feelings of aversion on a scale of 1-100.
 3. Smoking
In order to capture the dopamine response to a naturalistic smoking experience, instruct the smoker to smoke at his own pace, smoke his own brand of cigarettes, and most important, perform the smoking by himself, rather than have nicotine or the cigarette administered by study personnel. Smokers - who have been abstinent since the previous midnight - smoke two cigarettes in succession. They generally take about 10 min to complete both cigarettes.
 4. Rating scales post-smoking (as mentioned above).
 3. Post-PET scan
 1. Complete scan, send to reconstruction via MOLAR using Vicra data
After the acquisition is completed, reconstruct the list-mode data (a record of each individual decay event with its time and location) into emission images. The reconstruction algorithm used in our center is an iterative algorithm (Carson, Barker *et al.*²¹) that corrects for motion on the event level using the high-frequency Vicra recordings. Corrections for scatter, attenuation, dead-time, and normalization, scanner geometry, and point-spread-function are also included in the algorithm. The reconstruction produces a dynamic series of 3D PET images at pre-selected time-frames.
 2. MR pre-processing and MR-PET registration
Use standard algorithms to remove the skull from the subject's MR image²³. The MR must be de-skulled before aligning with PET because most tracers are not taken up by the skull.
 4. Filter the dynamic PET data with HYPR
Apply a variant of the spatial filtering method, Highly Constrained Backprojection (HYPR-LR) to all PET images in a frame-by-frame manner following the work of Christian *et al.*^{8,24}. The appeal of HYPR-LR is that it reduces spatial noise without degrading the temporal information at every voxel that we will use to create our dopamine movies.
 5. Align PET data to MR template
Align the PET to the subject's MR data to yield transformation matrix 1. (This is typically done with an image from early in the PET scan.) Register MR data to a standard MR template to yield transformation matrix 2. Combine transformations 1 and 2 to register the HYPR-filtered PET data to the standard template space. The data are now in a standard anatomical space with isotropic voxels (2 mm x 2 mm x 2 mm).
 6. Apply Striatal Mask
Raclopride has sufficient signal to background contrast to be used only in the striatum. This is the area of the brain that is implicated in drug addiction. Following Martinez *et al.*²⁵ apply a mask of the pre-commissural striatum (ventral striatum, dorsal caudate, dorsal putamen) to all the PET data in template space.
 7. Voxel-based fits of two models
 1. Select the dopamine response functions for lp-ntPET
Select response functions that are consistent with possible dopamine responses to the stimulus. By selecting a particular set of response functions, one can constrain the shape and timing of the estimated dopamine responses to curves that are expected for our particular stimulus. For smoking, we expect a unimodal rise and fall of dopamine concentration (a "gamma-variate" shaped curve). In the case of smoking at 45 min into the scan, families of response functions with "take-off" times of 40 min (to allow for some anticipation) and later are included.
 2. Apply the lp-ntPET model
Fit the lp-ntPET model to the PET TACs at each individual voxel in the masked region according to the method of Normandin *et al.*⁷. The operational equation of the model is shown in **Figure 3a**. The integral of the product of the PET TAC with each response function becomes a set of linear basis functions that contribute to the model (see last term in the operational equation). Because lp-ntPET is a linear, basis function-based method for fitting the dynamic PET data, it can be implemented to rapidly estimate both (a) kinetic parameters governing action of the tracer, and (b) a time-profile of relative dopamine concentration change during the scan session, at each voxel.
 1. Create WSSR maps
Record the weighted sum of squared residuals (WSSR) map of the fit of lp-ntPET to the data at each voxel ($\text{WSSR}_{\text{lp-ntPET}}$) for use, below. Fitting the model at each voxel produces images of the tracer parameters: R_1 , k_2 , k_{2a} , and γ . R_1 is the relative flow value, k_2 is the efflux rate in the reference region, k_{2a} is the apparent efflux rate in the target region, and γ is the magnitude of the dopamine signal. The weighted sum of squared residuals at each voxel can be thought of as an image as well.
 3. Apply the (conventional) Multilinear Reference Tissue Model (MRTM)

Fit the MRTM model following⁹ to the PET time-activity data at each individual voxel in the masked region. MRTM is a linear model - typically applied to dynamic PET data - that is identical to lp-ntPET *except that it lacks a time-varying dopamine term*. Fitting MRTM to voxel-wise data yields estimates of only three parametric images: R_1 , k_2 , k_{2a} . Record the weighted sum of squares map of the fit of MRTM ($WSSR_{MRTM}$) to the data at each voxel as well.

8. Calculate an F-map
Create an F-map from the sum of squares maps by calculating the F-statistic at each voxel in the mask. The F-statistic compares the $WSSR_{lp-ntPET}$ to the $WSSR_{MRTM}$, correcting for differences in degrees of freedom in the respective fits.
9. Threshold the F-map
Threshold the F-map at a value that translates to a probability of $p < 0.05$ (based on degrees of freedom in the model fits). The threshold is the same at every voxel. Binarize the map to make a new "Significance Mask" that retains only those voxels in the striatum whose PET TACs are fit (statistically) better with the lp-ntPET than with MRTM.
10. Filter the Significance Mask
Perform a morphological "opening" (erosion followed by dilation) on the Significance Mask to eliminate tiny, isolated clusters of voxels that we assume to be due to noise. An isotropic $2 \times 2 \times 2$ voxel kernel is used to remove isolated groups of voxels with diameters of 2 voxels or smaller. We now have a Final Significance Mask.
11. Create 4D dopamine movie in color
Store the value of the estimated dopamine curve normalized by k_{2a} at each voxel in the Final Significance Mask. These data constitute "normalized dopamine images" and will be 4-dimensional. They are, effectively, the relative dopamine value at each time-point for each voxel found to have a significant dopamine response to the stimulus. Create a color-coded image series by applying a color lookup table to the normalized dopamine images. Overlay the color-coded dopamine images on the corresponding MR template image. Save the series of color-coded images as a *.png file. This is a single-slice "dopamine movie". Arrange the dopamine movies for each slice containing ventral striatum into one movie. This arrangement is a multi-slice dopamine movie.
12. Analyze smoking data and control data similarly
Perform the same analysis on data from every experimental condition to be examined. For this project, we acquired and analyzed data for each subject in two separate conditions: smoking and control (no smoking).
13. Compare smoking to control by constructing a composite dopamine movie
Produce dopamine movies for the same subject in different conditions, e.g. baseline or sham task vs. smoking. Produce a "composite dopamine movie" for one subject for all slices of the striatum for baseline and smoking.
14. Run the movie
Play the "multi-slice dopamine movie" (shown in results) to reveal spatial and temporal patterns that comprise the brain's unique dopaminergic response to smoking cigarettes.

Representative Results

Figure 2. The effects of two different HYPR spatial filters on the smoothness of the time-activity data at a single striatal voxel. Top row: ^{11}C -raclopride PET emission images from a 3 minute frame centered at 46.5 minutes (not filtered, filtered with a $3 \times 3 \times 3$ voxel kernel, filtered by a $5 \times 5 \times 5$ voxel kernel). Middle row: ^{11}C -raclopride PET emission images from a 3 minute frame centered at 61.5 minutes (not filtered, filtered with a $3 \times 3 \times 3$ voxel kernel, filtered by a $5 \times 5 \times 5$ voxel kernel). Bottom row: Corresponding time activity curves from the same single voxel location in the left dorsal caudate. Note that the apparent dip in the ^{11}C -raclopride uptake (due to release of dopamine) at the time of smoking is preserved although the noise is diminished with greater filter size.

Figure 3. A selection of representative dopamine response functions that were pre-computed for fitting the lp-ntPET model to the PET time-activity data at each voxel according to Normandin *et al.*⁷. In the case of our smoking paradigm, cigarette smoking commences 45 minutes after tracer injection begins. Even if striatal dopamine responses encode anticipation of smoking - e.g. due to handling of the cigarette or other cues that foretell smoking - we reasoned that the response functions could safely be limited to curves that take off from baseline *no earlier* than 5 minutes prior to smoking (a). Similarly, curves were limited to take-off times *no later* than 15 minutes after start of smoking. Curves with take-off times at 40 minutes represent possible dopaminergic responses due to expectation. (b) Representative response functions all taking off from baseline at 45 minutes; the time when smoking commences. 500 different plausible response functions are generated. For illustration, plots in (a) and (b) show only a sampling of curve shapes and take-off times.

Figure 4. (a) The operational equation for the lp-ntPET model. The model is linear in parameters (R_1 , k_2 , k_{2a} , γ) which allows fast computation of parameter estimates at each voxel within the striatal mask. (b) Parametric images of (R_1 , k_2 , k_{2a} , γ) for a single coronal brain slice for a single subject. Although γ alone is the parameter that encodes the magnitude of a dopamine response, simultaneous estimation of all 4 tracer parameters is necessary to fit the model to the time-activity data at each voxel.

Figure 5. Fits of the conventional (MRTM) and new (lp-ntPET) models to the time-activity data from a voxel in the left caudate. MRTM fit is in blue. lp-ntPET fit is in red.

Figure 6. (a) shows the weighted sum of squared residuals (WSSR) from MRTM and (b) from lp-ntPET fits to the data at each striatal voxel. The two WSSR images produced from the same data are compared to produce a map of the F-ratio at each voxel (i.e. an F-map), shown in (c). (d) The F-map is thresholded at $p < 0.05$ to produce a binary significance map (see step 2.10 of the protocol). For n timeframes, and 4 parameters of the lp-ntPET model, the threshold for the F-statistic corresponding to a probability level, $p < 0.05$ (for 90 minutes of data binned in 3-minute frames, the threshold is 4.23) (e) The significance map is filtered with a morphological filter (an "opening") to eliminate tiny clusters of voxels that are most likely to represent noise. The Final Significance Mask preserves only those voxels in the striatum whose TACs are better fit (statistically) by the lp-ntPET model as opposed to the conventional MRTM model and thus are believed to contain a dopaminergic response to smoking. This threshold does not correct for multiple comparisons. Instead, to guard against false positive findings, we create Final Significance Masks for a control condition as well (see **Figure 7** and Protocol Steps 1.8 - 1.10).

Figure 7. (a) shows one coronal slice of the Final Significance Mask for the smoking condition in a single subject. Figure (b) shows the Final Significance Mask for corresponding subject and slice in the baseline condition. The presence of clusters of retained voxels in the mask of smoking as opposed to the *near-complete absence* of clusters in the mask of control supports the contention that the dopamine movies (see below) are not simply chance events or events related to noise in the data. (Note: the injected activity - and thus the signal to noise ratio - in the baseline and smoking conditions were comparable.)

Figure 8. The dopamine movie of a single slice of brain in the coronal orientation shows the frame-by-frame dopamine level relative to the basal (resting) dopamine level. (a) shows the movie of the baseline condition and (b) shows the movie of the smoking condition. The dopamine levels are encoded in color. Specifically, the colors - shown in the color bar with corresponding numerical values - represent the change in dopamine above the basal level as a percent of basal. Again, the dopamine levels are shown only for voxels in the Final Significance Mask that exceed the $p < 0.05$ significance level.

Figure 9. The multi-slice, multi-condition dopamine movie for the same subject as in **Figure 8** with all slices of the ventral striatum displayed simultaneously for baseline and smoking conditions.

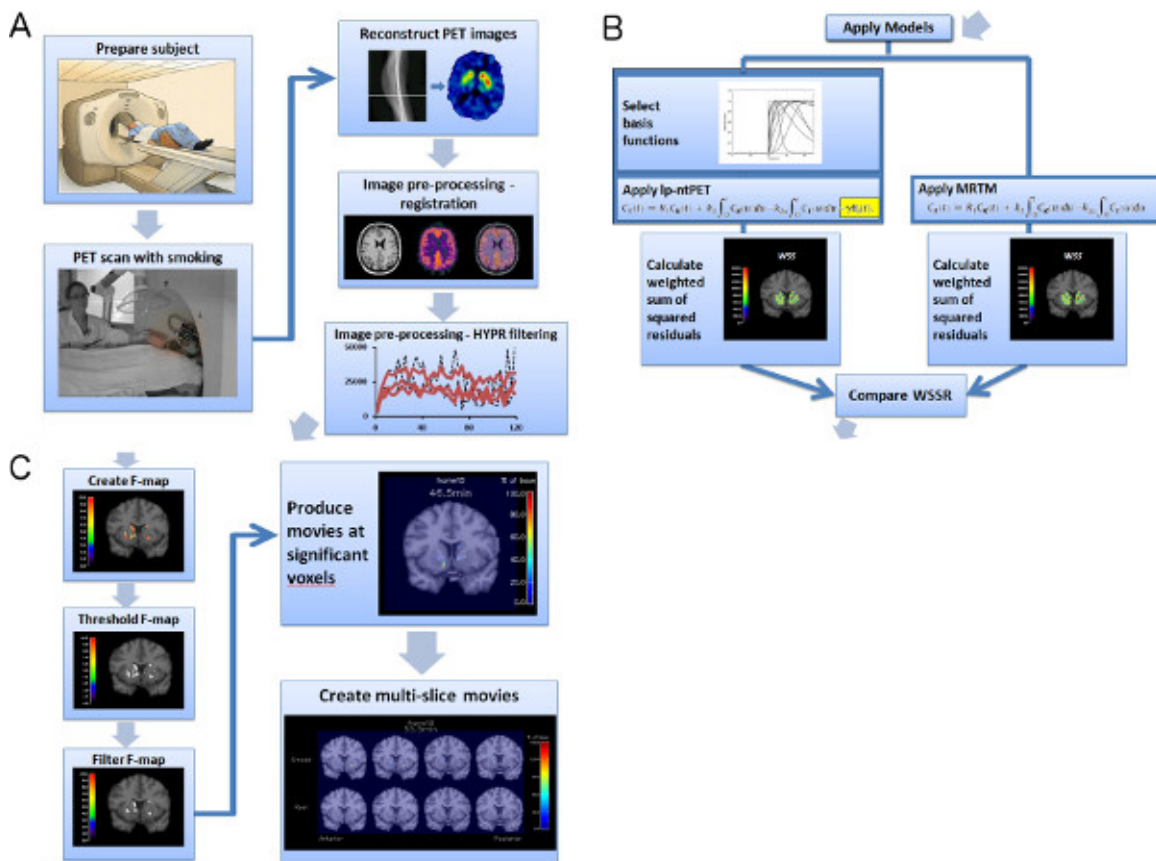


Figure 1. Flowchart of experiment and image analysis procedures (a-c). [Click here to view larger figure.](#)

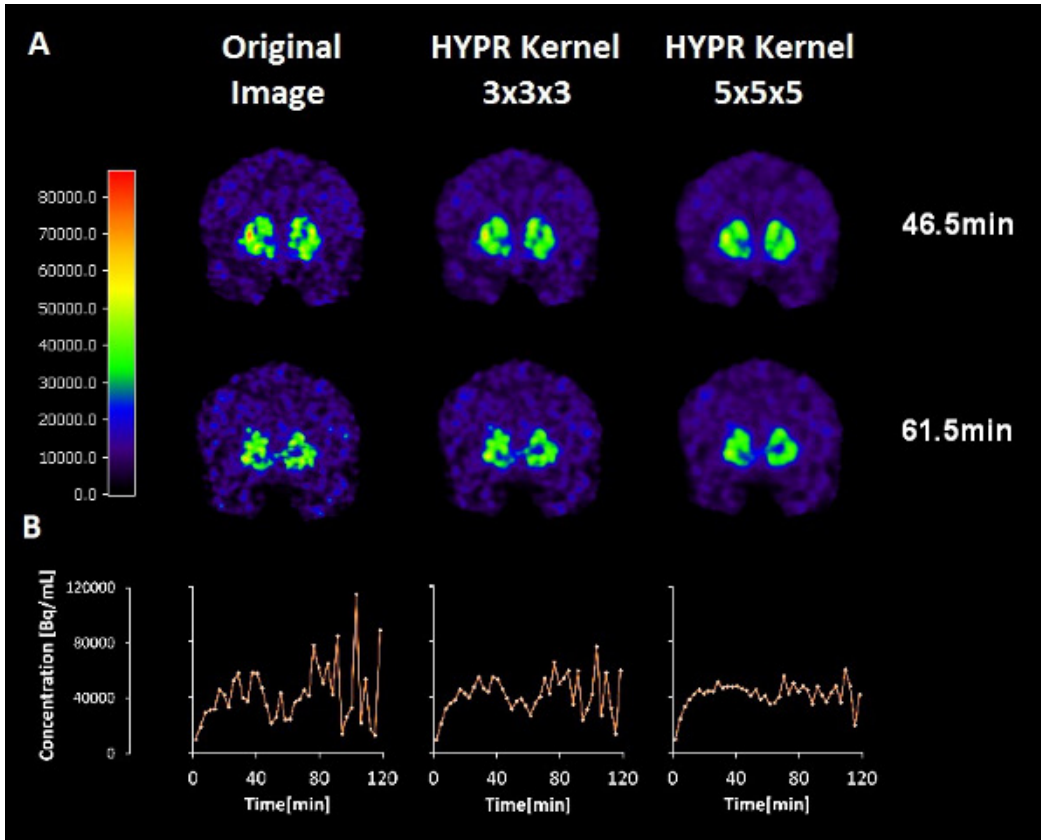


Figure 2. Effects of HYPR filters of different kernel size on images (top and middle) and on time activity curves (bottom) at a single voxel. [Click here to view larger figure.](#)

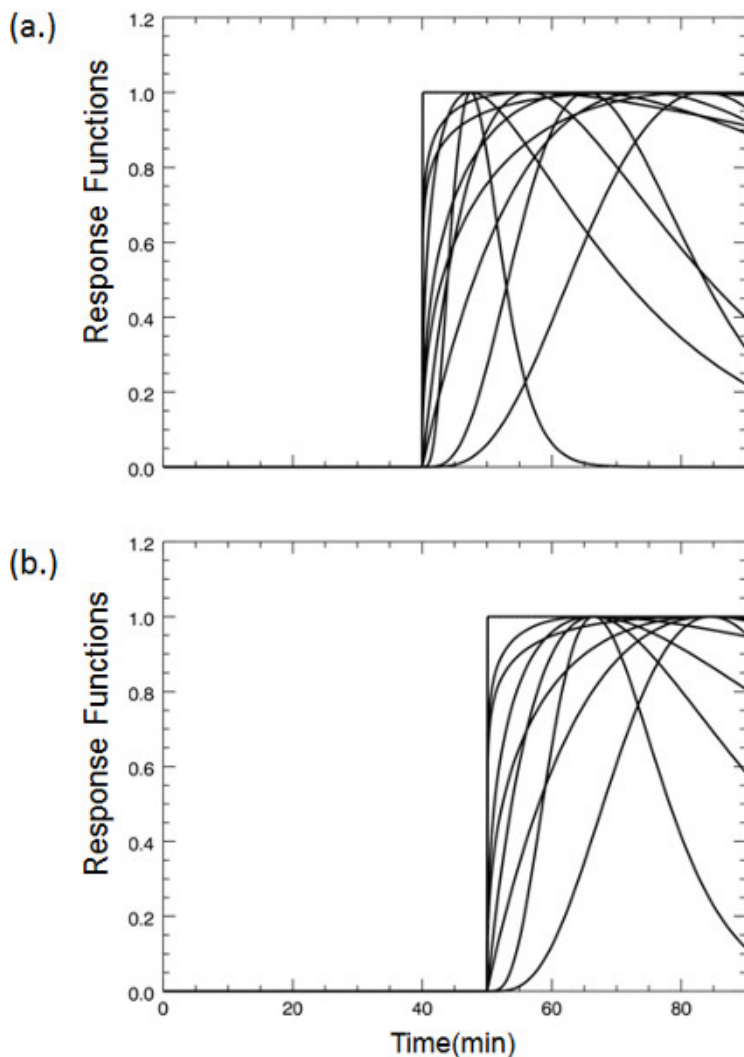


Figure 3. Examples of dopamine response functions that take-off at (a) 40 min or (b) 45 min post-tracer injection.

(a.)

$$C_T(t) = R_1 C_R(t) + k_2 \int_0^t C_R(u) du - k_{2a} \int_0^t C_T(u) du - \gamma B_i(t).$$

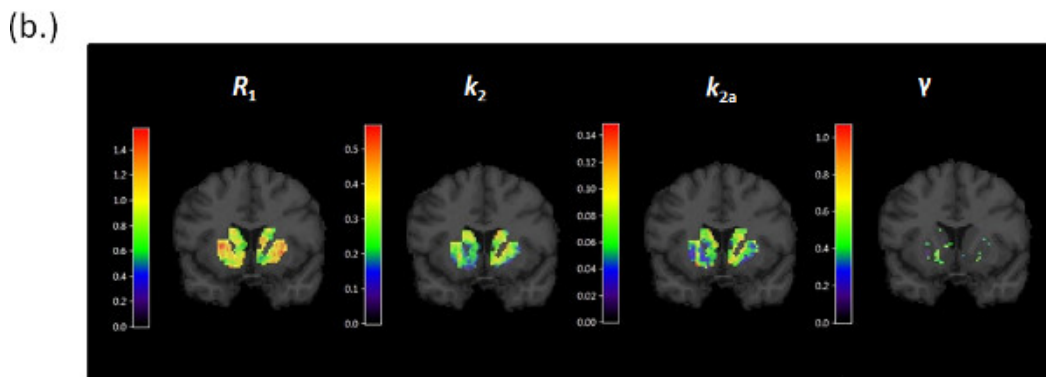


Figure 4. Parametric images generated by fitting the lp-ntPET operational equation (a) to the PET data. (b) Images corresponding to the 4 parameters of the model, R_1 , k_2 , k_{2a} , γ , are evaluated for the striatum and shown overlaid on the corresponding MR slice. [Click here to view larger figure.](#)

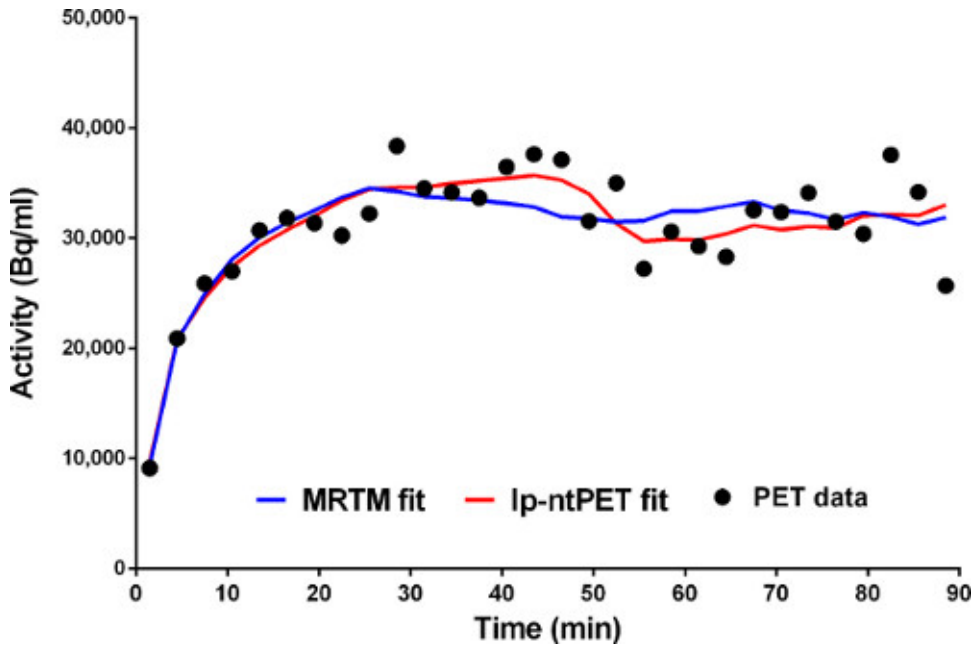


Figure 5. Fits of MRTM (blue) and Ip-ntPET (red) models to time-activity data from a single voxel.

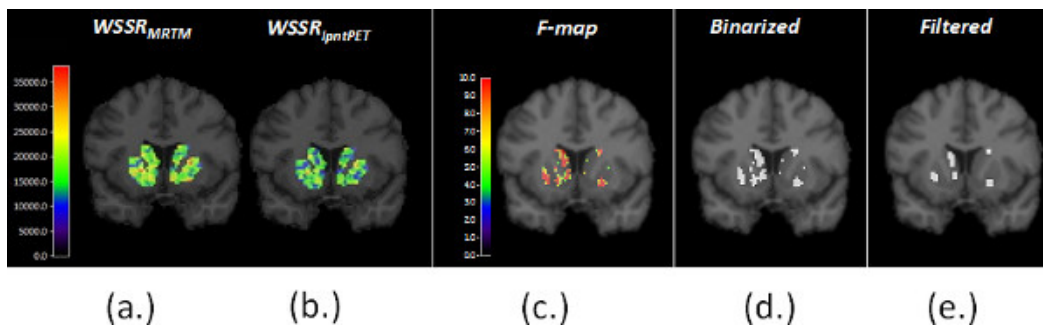


Figure 6. Parametric images of the WSSR for (a) MRTM and (b) Ip-ntPET. The respective WSSR maps are compared to create the F-map (c), which in turn is thresholded to a binary mask (d) and then filtered to produce the Final Significance Mask. [Click here to view larger figure.](#)

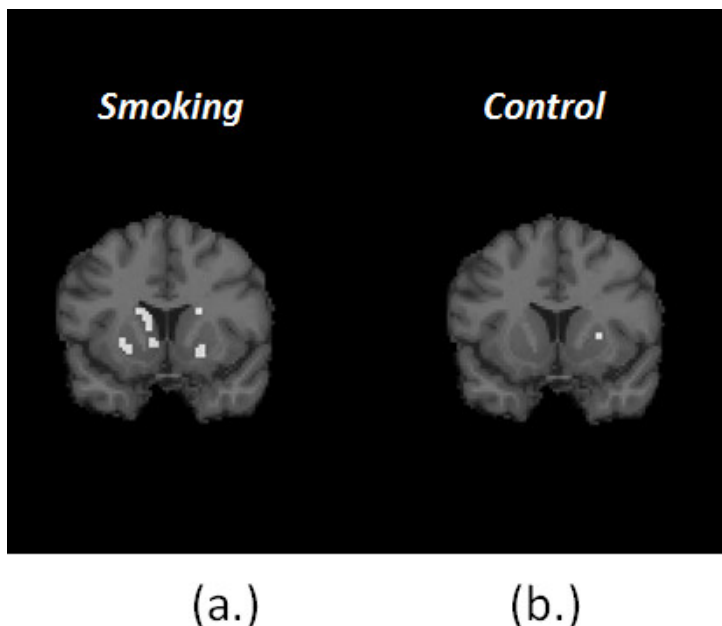


Figure 7. Comparison of Final Significance Masks for smoking (a) and control (b) conditions for the same subject.

Figure 8. Single-slice dopamine movie for single subject in control ('Rest') and smoking conditions. [Click here to view Figure 8.](#)

Figure 9. Multi-slice dopamine movie for single subject in (top) smoking and (bottom) control ('Rest') conditions. [Click here to view Figure 9.](#)

Discussion

Findings in the PET literature on the dopamine response to smoking are inconsistent¹³⁻¹⁸. There may be many reasons for this. Various methodological difficulties arise with any attempt to image cigarette smoking. At the very least, one must contend with possible motion artifacts in the data, second-hand smoke exposure for researchers, modest and short-lived changes in dopamine that cause only subtle alterations to the uptake and retention of the tracer, ¹¹C-raclopride.

Artificial induction of a large and sustained response of dopamine might be possible by administering an IV injection of a large dose of nicotine. However, this would be contrary to our underlying aims in creating dopamine movies of cigarette smoking. Our intent was to examine as carefully as possible the dopaminergic response to the entire behavior of smoking. In addiction research, an important distinction is made between passive administration of drugs to a subject and self-administration. Our aim was to image self-administration - a smoker smoking his/her own preferred brand of cigarette - in order to capture and characterize the brief dopaminergic response to smoking. PET analyses typically assume that the effects of a drug or other challenge are long-lived relative to the scan duration. Imaging smoking thus required innovations in modeling and in experimentation with PET.

Critical Steps in our protocol

Facilitating smoking in the scanner

1. In order to image self-administration (*i.e.* smoking) we had to eliminate second-hand smoke to the satisfaction of our Environmental Health and Safety department. This was accomplished through the use of a portable Air Filtration system which pulls the air surrounding the subject through a HEPA filter to remove particulate matter. The unit is equipped with a clear dome-shaped intake hood that can be lowered over the subject's face but not impede his/her smoking.
2. Smoking induces head motion - even if smokers are instructed to move their hand and keep their head still. Motion during a single time-frame degrades the point-spread function of the scanner. That is, it contributes to blur in the images. Head motion during scanning also means that the head is in different positions during emission and transmission. This mismatch can lead to artifacts when the transmission scan is applied to correct for attenuation. The Vicra head-tracking system addresses both of these issues and is generally considered to represent the state-of-the-art solution to the problem²⁶.

Maximizing sensitivity of ¹¹C-raclopride uptake to small changes in dopamine levels

3. Previous simulation work by our group has indicated that the sensitivity to changes in dopamine levels is not uniform throughout the scan duration if the tracer is administered *via* a bolus injection²⁷. On the other hand, an initial bolus of tracer followed by a slow infusion appears to greatly equalize the sensitivity of the PET data to smoking at any time during the scan.
4. Smoking-induced changes in dopamine are small relative to the noise in the PET data themselves. Highly Constrained Backprojection Reconstruction (HYPR)^{8,24} is a popular method of smoothing of fMRI data that has recently been applied to PET. This *spatial* smoothing technique reduces noise without obliterating the *temporal* characteristics of the data we are interested in. That is, the deflections in the time-activity curves that represent the competition of the tracer with endogenous dopamine. Our preliminary work²⁸ indicates that there is an optimal choice of HYPR filter that maximizes the difference in thresholded F-maps (*i.e.* difference in number of retained voxels) between smoking and baseline conditions. The optimal filter (chosen for the data presented) probably depends on proper matching of the HYPR kernel size to the approximate size of the activation area (See **Figure 2**).
5. Smoking-induced changes in dopamine are brief. Conventional PET analysis methods are not well-suited to the capture of transient neurotransmitter events^{25,29}. We have characterized the shortcomings of various conventional analyses using simulation studies and human data³⁰. For these reasons, our lab has developed and validated a number of mathematical techniques for modeling the effect of dopamine transients on PET data¹⁻⁷. A recent innovation by Normandin *et al.*⁷ was to linearize our original ntPET model so it could be applied at the voxel level. The result of doing so is a dopamine movie like the ones presented herein. Key aspects of our methods for estimating the dopamine transients in PET data have been validated previously: in rats undergoing simultaneous PET and microdialysis⁴ and in humans performing a finger tapping task^{3,4}.
6. Some sort of statistical test is required to isolate bonafide changes in dopamine as distinct from chance events. We have chosen to use the F-statistic (aka the "F-ratio") to identify the regions (*i.e.* the voxels) of the image that are most likely to contain detectable and quantifiable dopamine responses. The F-statistic is used to compare the sums of squares of the fits of two nested models to the same time-activity data. In this case, we compare the fit of a conventional model -absent a time-varying dopamine term- with our recently introduced lp-ntPET model that contains a time-dependent term for dopamine fluctuations. Only those voxels for which the F-ratio exceeds a given statistical threshold are retained in the final dopamine movie.

Limitations to the interpretation of the presented result

1. The sample result presented here is, of course, not a complete study. A thorough study of smoking would involve a baseline condition, a smoking condition, and a sham smoking condition to control for motion-induced dopamine release - as distinct from motion artifact (see above). These studies are ongoing in our laboratory. It should be noted that constructing an appropriate sham smoking condition is far from simple. For smokers, the mere act of bringing an unlit cigarette to their mouths may be rewarding and hence release dopamine. Thus, a control for motion but not for expectation would probably be a directed motor movement of comparable effort and frequency to taking puffs on a cigarette but not a movement that could not in any way be associated with smoking such as button pressing or manual object manipulation.

- It is well recognized that if enough comparisons are made, there will be chance findings that exceed a given statistical threshold³¹. The comparisons we are making are between the fit of the conventional model and the fit of the lp-ntPET model at all voxels in the striatum. At present, we are not correcting formally for multiple-comparisons (e.g. "Bonferroni correction"). Instead, we have applied the dopamine movie analysis to a baseline condition in addition to a smoking condition. If our dopamine movie of smoking were simply the result of chance, we would expect the same density of activation areas (number of supra-threshold voxels) in the baseline as in the smoking data. That is clearly not the case (see **Figure 7**).
- Certainly, the reproducibility of our technique is an important related issue. One would expect that the brain of a smoker should respond similarly to smoking a cigarette today or tomorrow or next week. We are presently engaged in assessing the test-retest reproducibility of our dopamine movies.

Future

We have developed a new model of PET tracer uptake in the presence of a short term fluctuation in endogenous neurotransmitter level. Because the model is linear in parameters, it can be computed quickly and easily at many voxels. The endpoint of fitting such a model to the PET data on a voxel-by-voxel basis is a "movie". For studies with the D2 receptor tracer, ¹¹C-raclopride, the endpoint is a *dopamine* movie. Dopamine is the key neurotransmitter involved in the brain's processing of rewarding stimuli that leads to addiction. Because some stimuli (most notably cigarettes and alcohol) produce only mild and probably short-lived dopamine changes, the movies may have their greatest potential for studying the abuse of these two stimuli. If we can use our dopamine movies to identify spatial and temporal patterns of dopamine release that are indicative of dependence or risk of abuse, then these patterns could serve as markers of disease, risk of disease, and - assuming the patterns are reversible - indicators of (pharmacological- or cognitive-) treatment efficacy.

There is nothing about our movies that restricts them to the dopamine system. All that is needed is a PET tracer for a target of interest that is sensitive to (*i.e.* easily displaceable by) fluctuations in the endogenous ligand for the same target. To date, there has been halting progress to identify PET tracers that are reliably sensitive to endogenous neurotransmitters other than dopamine. A review of the serotonin literature in 2010, for example, painted sobering picture of our current limited ability to detect serotonin release with PET³². Recently, there have been some encouraging developments. A number of publications have reported sensitivity of serotonin tracers to elevations in endogenous serotonin in non-human primates³³⁻³⁶ but the field awaits similar demonstrations in humans. As we have discussed elsewhere³⁷, sensitivity to changes in endogenous neurotransmitter concentration appear to be comprised of an optimal rate of displacement from the receptor combined with an ease of efflux of the tracer from tissue to blood. Once serotonin ligands have been validated and shown to have such properties, then serotonin movies will also be possible.

Presently, most PET studies with receptor-tracers lead to the generation of parametric images. A parametric image is a map of a given tracer kinetic model parameter evaluated at every voxel in the object (*i.e.* the brain). Application of conventional models such as SRTM^{38,39} or the one- or two-tissue compartment model yields parametric images of R_i , the regional flow parameter, or BP , the regional binding potential value. Both of these parameters are physiological constants that are believed to represent processes that are in steady state. Sometimes, however, the system and/or the process of interest are unsteady. That is, they are transient. Such is the case with the short-lived response of dopamine to cigarette smoking. In such circumstances, it is not possible to characterize the dopamine transient with a single parametric image. Nor is it appropriate to model the data with a model that is strictly time-invariant in parameters. There is a need for a model with a time-varying term to describe dopamine concentration changes in the striatum in response to smoking. The natural output of such a model when used with a dopamine tracer, is a movie of dopamine. This is a new form of functional image output that likely will spur and require new forms of analysis to maximize its utility.

Disclosures

All authors state that they have nothing to disclose.

Acknowledgements

The authors thank the members of the Yale PET Center chemistry team for tracer synthesis, the imaging team for tracer injection and image acquisition and Ms. Sheila Huang for expert flow-chart design.

Much of the development of the ntPET techniques was supported by R21 AA15077 to E. Morris. K. Cosgrove is supported by K02 DA031750.

References

- Constantinescu, C.C., Bouman, C., & Morris, E.D. Nonparametric extraction of transient changes in neurotransmitter concentration from dynamic PET data. *IEEE Trans. Med. Imaging*. **26**, 359-373 (2007).
- Constantinescu, C.C., *et al.* Estimation from PET data of transient changes in dopamine concentration induced by alcohol: support for a non-parametric signal estimation method. *Phys. Med Biol.* **53**, 1353-1367 (2008).
- Morris, E.D., Constantinescu, C.C., Sullivan, J.M., Normandin, M.D., & Christopher, L.A. Noninvasive visualization of human dopamine dynamics from PET images. *NeuroImage*. **51**, 135-144 (2010).
- Morris, E.D., Normandin, M.D., & Schiffer, W.K. Initial comparison of ntPET with microdialysis measurements of methamphetamine-induced dopamine release in rats: support for estimation of dopamine curves from PET data. *Molecular imaging and biology : MIB : the official publication of the Academy of Molecular Imaging*. **10**, 67-73 (2008).
- Morris, E.D., *et al.* ntPET: a new application of PET imaging for characterizing the kinetics of endogenous neurotransmitter release. *Molecular Imaging*. **4**, 473-489 (2005).
- Normandin, M.D., & Morris, E.D. Estimating neurotransmitter kinetics with ntPET: A simulation study of temporal precision and effects of biased data. *NeuroImage*. **39**, 1162-1179 (2008).

7. Normandin, M.D., Schiffer, W.K., & Morris, E.D. A linear model for estimation of neurotransmitter response profiles from dynamic PET data. *NeuroImage*. **59**, 2689-2699 (2012).
8. Christian, B.T., Vandehey, N.T., Floberg, J.M., & Mistretta, C.A. Dynamic PET denoising with HYPR processing. *Journal of Nuclear Medicine: Official publication, Society of Nuclear Medicine*. **51**, 1147-1154 (2010).
9. Ichise, M., et al. Linearized reference tissue parametric imaging methods: application to [11C]DASB positron emission tomography studies of the serotonin transporter in human brain. *Journal of cerebral blood flow and metabolism : official journal of the International Society of Cerebral Blood Flow and Metabolism*. **23**, 1096-1112 (2003).
10. Benowitz, N.L. Pharmacology of nicotine: addiction, smoking-induced disease, and therapeutics. *Annual review of pharmacology and toxicology*. **49**, 57-71 (2009).
11. Volkow, N.D., & Swanson, J.M. Variables that affect the clinical use and abuse of methylphenidate in the treatment of ADHD. *The American journal of psychiatry*. **160**, 1909-1918 (2003).
12. Di Chiara, G., & Imperato, A. Drugs abused by humans preferentially increase synaptic dopamine concentrations in the mesolimbic system of freely moving rats. *Proc. Natl. Acad. Sci. U.S.A.* **85**, 5274-5278 (1988).
13. Barrett, S.P., Boileau, I., Okker, J., Pihl, R.O., & Dagher, A. The hedonic response to cigarette smoking is proportional to dopamine release in the human striatum as measured by positron emission tomography and [11C]raclopride. *Synapse*. **54**, 65-71 (2004).
14. Brody, A.L., et al. Gene variants of brain dopamine pathways and smoking-induced dopamine release in the ventral caudate/nucleus accumbens. *Arch. Gen. Psychiatry*. **63**, 808-816 (2006).
15. Brody, A.L., et al. Smoking-induced ventral striatum dopamine release. *The American journal of psychiatry*. **161**, 1211-1218 (2004).
16. Montgomery, A.J., Lingford-Hughes, A.R., Egerton, A., Nutt, D.J., & Grasby, P.M. The effect of nicotine on striatal dopamine release in man: A [11C]raclopride PET study. *Synapse*. **61**, 637-645 (2007).
17. Scott, D.J., et al. Smoking modulation of mu-opioid and dopamine D2 receptor-mediated neurotransmission in humans. *Neuropsychopharmacology: official publication of the American College of Neuropsychopharmacology*. **32**, 450-457 (2007).
18. Takahashi, H., et al. Enhanced dopamine release by nicotine in cigarette smokers: a double-blind, randomized, placebo-controlled pilot study. *Int. J. Neuropsychopharmacol.* **11**, 413-417 (2008).
19. Morris, E.D., Fisher, R.E., Alpert, N.M., Rauch, S.L., & Fischman, A.J. In vivo imaging of neuromodulation using positron emission tomography: Optimal ligand characteristics and task length for detection of activation. *Human Brain Mapping*. **3**, 35-55 (1995).
20. Alpert, N.M., Badgaiyan, R.D., Livni, E., & Fischman, A.J. A novel method for noninvasive detection of neuromodulatory changes in specific neurotransmitter systems. *NeuroImage*. **19**, 1049-1060 (2003).
21. Carson, R.E., Barker, W.C., Jehi-San, L., & Johnson, C.A. In: *Nuclear Science Symposium Conference Record, 2003 IEEE.*, Vol. **3285.**, 3281-3285 (2003).
22. Carson, R.E., et al. Comparison of bolus and infusion methods for receptor quantitation: application to [18F]cyclofoxy and positron emission tomography. *Journal of cerebral blood flow and metabolism : official journal of the International Society of Cerebral Blood Flow and Metabolism*. **13**, 24-42 (1993).
23. Smith, S.M. Fast robust automated brain extraction. *Human brain mapping*. **17**, 143-155 (2002).
24. Floberg, J.M., et al. Improved kinetic analysis of dynamic PET data with optimized HYPR-LR. *Medical physics*. **39**, 3319-3331 (2012).
25. Martinez, D., et al. Imaging human mesolimbic dopamine transmission with positron emission tomography. Part II: amphetamine-induced dopamine release in the functional subdivisions of the striatum. *Journal of cerebral blood flow and metabolism : official journal of the International Society of Cerebral Blood Flow and Metabolism*. **23**, 285-300 (2003).
26. Montgomery, A.J., et al. Correction of head movement on PET studies: comparison of methods. *Journal of nuclear medicine : official publication, Society of Nuclear Medicine*. **47**, 1936-1944 (2006).
27. Yoder, K.K., Wang, C., & Morris, E.D. Change in binding potential as a quantitative index of neurotransmitter release is highly sensitive to relative timing and kinetics of the tracer and the endogenous ligand. *Journal of nuclear medicine : official publication, Society of Nuclear Medicine*. **45**, 903-911 (2004).
28. Wang, S., et al. In: *The 9th International Symposium on Functional Neuroreceptor Mapping of the Living Brain.*, NRM12, (2012).
29. Ginovart, N. Imaging the dopamine system with in vivo [11C]raclopride displacement studies: understanding the true mechanism. *Molecular imaging and biology : MIB : the official publication of the Academy of Molecular Imaging*. **7**, 45-52 (2005).
30. Sullivan, J.M., Kim, S.J., Cosgrove, K.P., & Morris, E.D. In: *The 9th International Symposium on Functional Neuroreceptor Mapping of the Living Brain*. NRM12, (2012).
31. Miller, R.G. *Simultaneous Statistical Inference 2nd Ed.* (1981).
32. Paterson, L.M., Tyacke, R.J., Nutt, D.J., & Knudsen, G.M. Measuring endogenous 5-HT release by emission tomography: promises and pitfalls. *Journal of cerebral blood flow and metabolism : official journal of the International Society of Cerebral Blood Flow and Metabolism*. **30**, 1682-1706 (2010).
33. Ridler, K., et al. Characterization of in vivo pharmacological properties and sensitivity to endogenous serotonin of [11C] P943: a positron emission tomography study in *Papio anubis*. *Synapse*. **65**, 1119-1127 (2011).
34. Cosgrove, K.P., et al. Assessing the sensitivity of [(1)(1)C]p943, a novel 5-HT1B radioligand, to endogenous serotonin release. *Synapse*. **65**, 1113-1117 (2011).
35. Finnema, S.J., et al. Fenfluramine-induced serotonin release decreases [11C]AZ10419369 binding to 5-HT1B-receptors in the primate brain. *Synapse*. **64**, 573-577 (2010).
36. Finnema, S.J., Varrone, A., Hwang, T.J., Halldin, C., & Farde, L. Confirmation of fenfluramine effect on 5-HT(1B) receptor binding of [(11)C]AZ10419369 using an equilibrium approach. *Journal of cerebral blood flow and metabolism : official journal of the International Society of Cerebral Blood Flow and Metabolism*. **32**, 685-695 (2012).
37. Morris, E.D., & Yoder, K.K. Positron emission tomography displacement sensitivity: predicting binding potential change for positron emission tomography tracers based on their kinetic characteristics. *Journal of cerebral blood flow and metabolism : official journal of the International Society of Cerebral Blood Flow and Metabolism*. **27** (2007).
38. Gunn, R.N., Lammertsma, A.A., Hume, S.P., & Cunningham, V.J. Parametric imaging of ligand-receptor binding in PET using a simplified reference region model. *NeuroImage*. **6**, 279-287 (1997).
39. Lammertsma, A.A., et al. Comparison of methods for analysis of clinical [11C]raclopride studies. *Journal of cerebral blood flow and metabolism : official journal of the International Society of Cerebral Blood Flow and Metabolism*. **16**, 42-52 (1996).